IV International Conference on Simulation for Additive Manufacturing
Sim-AM 2023
E. Rank and S. Kollmannsberger (Eds)

EFFECT OF RESIDUAL STRESSES ON THE MECHANICAL PROPERTIES OF ADDITIVE MANUFACTURED TPMS LATTICE STRUCTURES MADE OF STAINLESS STEEL

HRUSHIKESH S. MAPARI[*], HENRIK KRUSE[†], DR. ENRIQUE ESCOBAR DE OBALDIA[*], DR. ALEXANDRE MATEI[#] AND DR. JOHANNES H. SCHLEIFENBAUM[†]

[*] Ansys Germany GmbH
Staudenfeldweg 20, 83624 Otterfing, Germany
e-mail: hrushikesh.mapari@ansys.com, enrique.escobar@ansys.com

[†] Digital Additive Production DAP, RWTH Aachen University
Campus-Boulevard 73, 52074 Aachen, Germany
e-mail: henrik.kruse@dap.rwth-aachen.de

[#] Ansys France
15 Pl. Georges Pompidou, 78180 Montigny-le-Bretonneux, France
e-mail: alexandre.matei@ansys.com

Key words: Residual stresses (RS), Additive manufacturing (AM), Laser Powder Bed Fusion (PBF-LB/M), Finite Element Modelling (FEM), numerical modeling

Abstract. In recent years, the use of Triply Periodic Minimal Surface (TPMS) lattice structures has gained popularity due to their advantages like high surface to volume ratio and their lightweight potential. Nowadays, TPMS lattice structures can be seen in many fields, including aerospace and medical applications, which can be fabricated using AM methods like Laser Powder Bed Fusion (PBF-LB/M) process. During the PBF-LB/M process, the transient temperature change is caused by the cyclic nature of the thermal load resulting in the accumulation of residual stresses (RS). These RS can cause dimensional inaccuracies, warpage and have a severe impact on the loading capacity and quality of the PBF-LB/M part.

In this paper, the effect of RS on the mechanical properties of primitive and gyroid TPMS lattice structures of volume fraction 20%, 30% and 40% undergoing compression testing is studied using Finite Element Analysis (FEA) and experiments. The sequentially coupled thermomechanical finite element model is used to account for the RS accumulation and its effect on Young's modulus, yield strength and Specific Energy Absorption (SEA).

It is seen that the RS have a detrimental effect on all three considered properties of additively

manufactured lattices. The primitive structure of 20% volume fraction shows significant softening, which is aggravated by the RS. The yield strength and Young's modulus of primitive structure increase with increasing volume fraction, but the values of the simulation with RS are considerably lower than those without RS. A similar reduction in values of the properties is found in gyroid structures, but the effect of volume fraction is not significant, with values remaining in a similar range. Regarding SEA which is calculated up to 20% strain, the primitive structure performs better than the gyroid, except in the case of 20% volume fraction, where the SEA value of the primitive is less than the gyroid due to the softening.

1 INTRODUCTION

Lattice structures exhibit numerous attractive properties, such as high strength, high energy absorption capacity, vibration mitigation, thermal conductivity, and low mass [1, 2]. These properties have made lattice structure integration in structures a point of research in many fields like automotive, aerospace and biomedical applications [2]. With laser powder bed fusion (PBF-LB/M), one of the most widespread AM technologies, it is possible to produce such lattices with high control over the cell size, topology, and porosity.

Studies regarding the comparison of the mechanical properties of different types of lattice structures show that the properties stiffness, plateau stress and energy absorption of triply periodic minimal surface (TPMS) lattice structures are superior to other types of lattice structures like body-centred cubic (BCC) [3].

In PBF-LB/M, the successive melting and solidification of metal powder layers enable the manufacturing of these complex structures. During this process, the material undergoes repeated thermal cycles, leading to temperature gradients and non-uniform thermal expansion and contraction, which ultimately results in the accumulation of RS in the component [4]. The RS can cause cracking, dimensional inaccuracies and have a severe negative impact on the loading capacity and performance of the part [5]. Although the mechanical properties of the TPMS lattice structures have been studied by many researchers, the effect of RS on their mechanical properties remains largely unexplored [6].

RS are stresses which are confined inside the body and are in an equilibrium state when no external load is being applied, i.e., they are not required to maintain equilibrium between the body and the environment. In this paper, the RS considered act over a length scale of the size of the component, which usually appear when the material is processed thermally or mechanically. These are the stresses inside the body which are not necessary to maintain equilibrium between the body and its environment, also known as macrostress [7]. The evaluation of the RS becomes more complicated with the increasing complexity of the structure under consideration [8] and experimental measurements of RS are expensive and time-consuming [9]. Hence, finite element methods to simulate the RS are important.

The presence of RS can cause significant distortion and cracking of the part in thin-walled and complex structures such as lattices. RS influence the mechanical properties but are often left as an unknown factor in the design of such parts. There are studies regarding the experimental or computational determination of RS in AM structures [8], and even fewer regarding the effect of RS on the mechanical properties of lattice structures. Gan et al. established a simulation model for Ti-6AL-4V lattice structures manufactured using PBF-LB/M based on the inherent strain method and studied the effects of geometric lattice

parameters on the residual deformation and stress. It is concluded that the maximum RS decreases with the increase of rod angle and increases with the increase of rod diameter. Also, the residual deformation increased linearly with rod diameter [10]. Bruggeman conducted thermomechanical RS simulations for both simplified geometries, such as cubes and plates, and five complex lattice geometries fabricated using PBF-LB/M with Inconel 718. The numerical RS results of the lattice geometries show that the lattice geometries play a significant role in the distribution and magnitude of RS [11]. Ahmed et al. conducted simulations of the fabrication of four different types of TPMS lattice structures using a sequentially coupled thermo-mechanical finite element model to evaluate RS during the PBF-LB/M process. These results are used to obtain the mechanical properties of TPMS lattice structures while considering the effect of RS. The study concluded that the effective elastic modulus of all TPMS lattices in the build direction is lower in comparison with the reference TPMS in which the RS are not accounted for [12].

As discussed, FEA has been used to measure the accumulation of RS and mechanical properties of TPMS lattices separately, but few studies have been conducted to simulate the effect of RS on the mechanical properties of the TPMS lattices and compare them with the experiments. Therefore, in this paper, a methodology to simulate the accumulation of the RS and their effect on the three key mechanical properties (Young's modulus, yield strength and specific energy absorption) of two TPMS lattices (primitive and gyroid) is presented. The FEA results are compared with the experimental results.

2 METHODOLOGY AND IMPLEMENTATION

2.1 Design of compression test specimen

The design of the test specimens was done based on two standards, DIN 50134 and ISO 13314. Specimens with three different volume fractions – 20%, 30%, and 40% were designed to study the effect of volume fraction on the properties. The designed specimens of primitive and gyroid of volume fraction 20% are shown in Figure 1. The volume fraction is calculated as follows:

$$Volume\ fraction\ [\%] = \frac{Volume_l}{Volume_c} \times 100 \tag{1}$$

where $Volume_l$ is the volume of the lattice structure and $Volume_c$ is the volume of the cuboid enclosing the given lattice structure. The specimens were cuboid in shape, with the ratio of edge length to height set to 1.5. The size of the compression specimen was 35 mm×35 mm×52.5 mm, with the size of the unit cell as 3.5 mm×3.5 mm×3.5 mm. To avoid damaging the lattice structure while removing it from the baseplate, the bottom surface of the lattice was extruded by 2 mm as seen in Figure 1. These specimens were designed using the TPMS lattice option in Ansys Material Designer. The wall thickness for each volume fraction and the total volume of each specimen from the CAD models is given in Table 1.

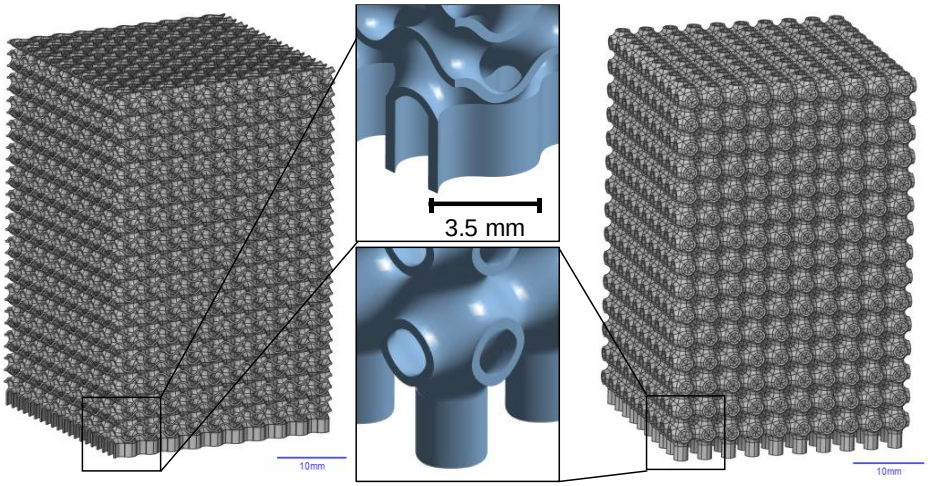

Figure 1: Compression test specimen of gyroid (left) and primitive (right) with volume fraction 20%

Table 1: Compression test specimen design data

Lattice type	Primitive			Gyroid		
Volume fraction [%]	20	30	40	20	30	40
Wall thickness [mm]	0.3	0.45	0.61	0.23	0.34	0.46
Lattice volume [mm^3]	12831	19264.5	25705.5	12834	19255.5	25686

2.2 Machine setup and calibration

The compression test specimens were fabricated from stainless steel 316L on a commercial PBF-LB/M machine (EOS M 290). The process parameters of the machine used for the fabrication are listed in Table 2.

Table 2: Machine parameters for the fabrication using PBF-LB/M

Process parameter	Laser power [W]	Deposition thickness [mm]	Hatch spacing [mm]	Laser speed [mm/s]	Preheat temperature [°C]	Room temperature [°C]
Value	120	0.03	0.08	800	35	20

A distortion calibration procedure for the simulation based on the physical manufacturing scenario is highly recommended to determine the Thermal Strain Scaling Factor (TSSF) to use in Ansys thermal-structural simulations [13]. The calibration procedure was performed using cantilever specimens in the same conditions as the main study.

Four compression testing specimens of each type (primitive and gyroid) were fabricated and tested. The specimens were separated from the base plate using wire electro-erosion and underwent ultrasound vibration to remove the remaining powder particles inside the lattice voids and powder particles stuck to the lattice walls. To retain the accumulated RS to investigate their effect on the mechanical properties, the post-processing heat treatment was not carried out. Compression tests are performed on the as-built specimens.

The machine used for testing was a Z250 AllroundLine (ZwickRoell GmbH & Co. KG) with

a maximum load capacity of 250 kN. For the compression tests, the DIN 50134 standard is followed. The tests are carried out at room temperature under a constant strain rate of 0.001/s till 40% of the compression and with 0.01/s up to a maximum compression of 55%. The strain rate is increased to shorten the duration of the experiment.

2.3 Simulation setup for the PBF-LB/M and compression testing

The simulation is carried out in Ansys 2023R1. For additive manufacturing, a sequential thermal-structural model is followed, where a layer-by-layer simulation of thermal phenomena is performed first, and afterwards, those temperature results are used in the structural simulation.

For the AM simulations, the material data of 316L from the Ansys engineering data resources is used, with bilinear isotropic hardening. The geometry is meshed using layered tetrahedrons. Along with the process parameters listed in Table 2, standard values are used for the other required parameters for the simulation. The newly determined TSSF factor (from the calibration process) is used for the simulation. After entering the parameters, a step to remove the base plate and the extrusions is added. Additional commands are added in the structural simulation to save the database file and initial state files to store the deformation and stress data after the removal step so that they can be used as initialization files for the compression testing. For the simulation, a quarter part of the complete specimen (lattice structure with 5×5×15 unit cells) is used with the symmetry conditions to reduce the computational efforts.

After the completion of the thermal-structural simulation of the PBF-LB/M process, the database file is imported using an external data block to get the deformed lattice structure as geometry. Then, the initial state file is read in the first step to map the RS on the geometry. For the second step, the bottom face of the lattice is fixed, and displacement is applied to the top face of the lattice to mimic the compression test, with auto time stepping and large deflection options activated. As per the thermal-structural simulation, a quarter geometry is used for the compression test as well to reduce the computational effort. A compression test simulation without mapping any RS is also performed to check the mechanical properties without the effect of RS.

The directional displacement in the Z direction and reaction force on the top face are obtained as results from the simulation to get the force-displacement data. The force values are divided by the area of the top face, and displacement values are divided by the total height of the specimen to get the stress-strain data for the individual lattice type. This data is used to calculate the values of Young's modulus, yield strength, and specific energy absorption (SEA).

3 RESULTS AND DISCUSSION

3.1 TSSF, Deformation and residual stress using simulation of the AM process

In this section, the TSSF value found from calibration, deformation, and RS distribution in the specimens after removal from the base plate from the simulation are discussed.

The average distortion of the cantilever in calibration is found to be 0.76 mm and from the calibration process, the TSSF value is found out to be 0.062. After fabrication, the weight of the fabricated specimen was measured, and it was found that on average, the primitive specimens were 11.09% heavier and the gyroid specimens were 16% heavier than the CAD

models. This is similar to [14] where sheet-based TPMS lattices showed higher weight compared to their CAD models, which can be related to the surface area of the unit cell topology. As the surface area increases, so does the interaction between solidified structure and the powder bed, which leads to the additional weight of the final sample [14].

The deformation and accumulated stress in the quarter model with the applied symmetry boundary conditions of primitive and gyroid 20% volume fraction is shown in Figure 5. The coordinate system is set at the center of the cuboid and the part enclosed in the positive X, Y, and Z axis is modelled with symmetry boundary conditions on XZ and YZ planes, as shown in Figure 5(a). Images of the 20% volume fraction are shown as representatives, as the deformation and stress distribution in the 30% and 40% volume fraction is very similar.

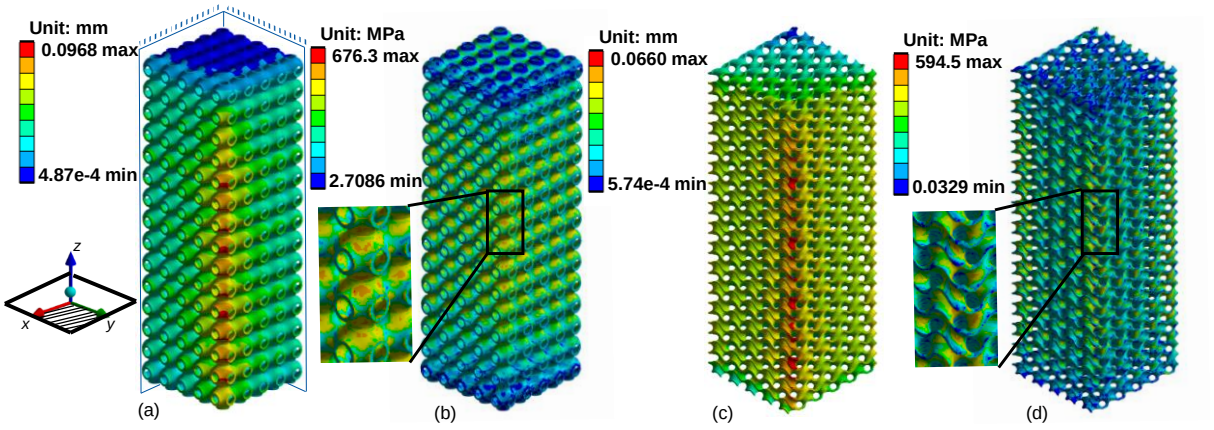

Figure 5: (a) Deformation and (b) stress distribution in the quarter primitive 20% and (c) deformation and (d) stress distribution in the quarter gyroid 20% specimen obtained from thermal-structural simulation

It can be seen from the images that the deformation and the distribution of RS are dependent on the topology of the lattice structure. In the case of the primitive structure, the deformation is lowest in the central part of the cuboid (around the Z-axis) and increases towards the outer edges of the structure. The maximum deformation is seen on the unit cells on the corner edge of the cuboidal lattice specimen. The stress distribution is not only non-uniform in the vertical direction across the whole body but also across the height of a single unit cell. It is important to note that the highest amount of stress accumulation is seen in the region where the unit cells are joined with each other, as seen in the zoomed-in section. Like the displacement, the value of RS is seen to be highest on the unit cells on the corner edge.

The overall deformation distribution in the gyroid lattice is similar to that of the primitive lattice. The lowest deformation is seen in the central region of the lattice around the Z-axis and increases gradually towards the outer faces. The highest stress accumulation is seen on the edges of the outer faces of the cuboid specimen. Unlike primitive, the stress distribution within the unit cell is more uniform. The topology of the gyroid unit cell is such that the unit cells are not very distinctly separated from each other and connected with multiple faces, whereas the primitive unit cells are connected via a single face with a comparatively smaller area, and distinctly separable. This is a possible reason for the more uniform RS distribution in the gyroid lattice structure.

This stress distribution in the cuboid specimens follows a similar pattern as discussed in the

literature regarding stress distribution in the vertical (along the Z-axis) and horizontal (along the X- and Y-axis) direction of plate specimens. Considering the build in Z direction, the shrinkage of the newly added layers after solidification causes the underlying layers to be compressed, and new layers show tensile stress. When further new layers are added, compressive stress within underlying layers increases. In this process, heat accumulates in the formed layers, reducing the thermal gradient. Hence, the stress shows a trend of decreasing near the top layers [15]. However, removal from the base plate causes a change in the stress state, and some stress is relieved [16]. This leads to the pattern of low stress in the lower and upper regions (blue colored), and higher stress in the central region (green-orange colored). Also in the horizontal plane, the scan vector geometry can have a localized heating effect, resulting in excess heat build-up within localized regions like the corners of the rectangular geometry [17]. This can be the reason behind the high stress accumulation on the corners of the specimens. As discussed earlier, there are very few studies regarding the distribution of RS in the TPMS lattice. Also, the parameters of the fabrication, size of the lattices and simulation procedure affect the stress values to a high degree. However, the general stress distribution tendency can be compared with the few studies available. Gan et al. concluded that the deformation in BCC lattices increases with the rod diameter, which aligns with the result of increasing deformation with increasing wall thickness in both primitive and gyroid lattices. Both Bruggeman [11] and Ahmed et al. [12] show that the distribution of RS is dependent on the unit cell topology. These studies also observe that the RS are non-uniformly distributed in vertical direction [12], the highest RS is observed on the central region of the corner edges, followed by the outer faces of the specimen and the least in the centre [11].

The graphical representation of the maximum deformation and maximum RS values is shown in Figure 6.

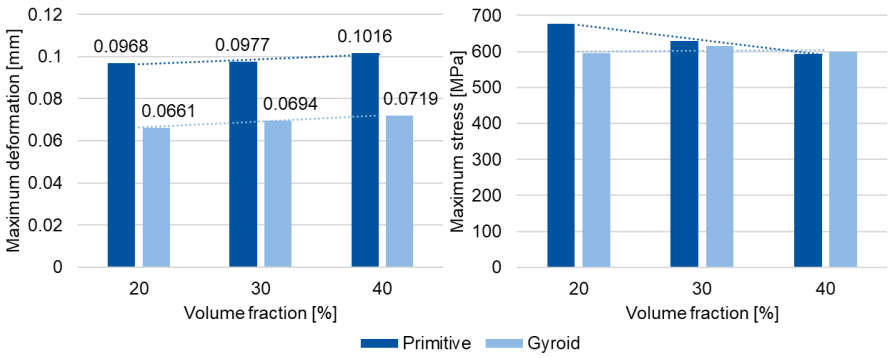

Figure 6: Maximum deformation and maximum stress in primitive and gyroid specimens obtained by simulation

The maximum deformation increases with increasing volume fraction for both primitive and gyroid structures, but the maximum deformation is approximately 30% higher in primitive than in gyroid structures for every volume fraction. For RS, in the case of primitive structures, there is a clear reduction in the maximum RS value with increasing volume fraction. The maximum RS decreases by nearly 12% from volume fraction 20 to 40%. However, in the case of gyroid structures, the maximum RS values are comparable with each other for all three volume fractions with a maximum difference between the values in the range of 3%. As discussed

earlier, the more uniform stress distribution in the gyroid can be the reason for the low variation in the maximum RS values. Contrary to that, the primitive lattices show clear areas of stress concentrations, leading to a clear decreasing trend.

3.2 Compression test results

The representative images of 20% volume fraction specimens of primitive and gyroid after undergoing compression and the stress-strain characteristics for all the tested specimens are shown in Figure 7. The curves for all the specimens are very close to each other in the elastic region, and therefore a closer look is needed to differentiate Young's modulus value for primitive and gyroid for different volume fractions, which is done in the next section. For the primitive lattice, after the elastic region, there is a clear distinction between the behavior of the different volume fractions. The yield strength of the primitive lattice increases with the increasing volume fraction. The 20% volume fraction lattice structure shows very little increase in stress up to 10% strain, indicating very little hardening of the sample.

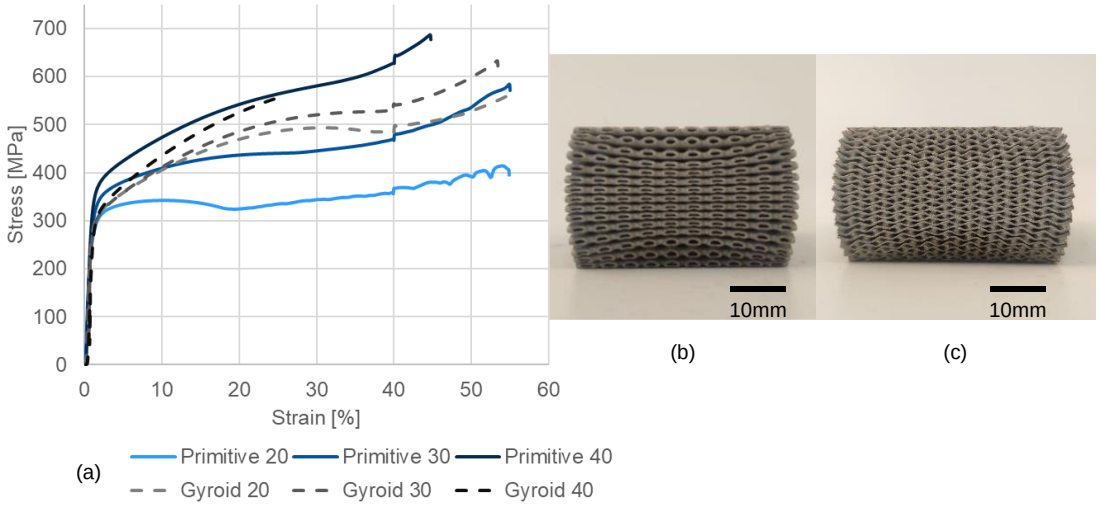

Figure 7: (a) Stress-strain graphs of compression testing, compressed specimens of (b) primitive 20% and (c) gyroid 20% structures

In addition, after 10% strain, it shows strong softening up until 20% strain, which is particular to this lattice. At this point, the slope of the curve again changes direction, and stress starts to increase. This can be attributed to the self-contact between the lattice cell walls and is known as densification. The primitive 20% lattice starts the densification at the earliest at 20% strain. Some fluctuations in the stress-strain curve can be seen at the very end around 50% compression, which can be attributed to the collapse of some unit cells at the center of the specimen. The 30% and 40% primitive specimens show hardening until 25-40% strain and start showing significant densification after that. Due to the initial difference in the yield strength, the overall curve of the 40% volume fraction shows higher stress values, but the hardening and densification are similar to the 30% specimen.

In the case of the gyroid lattice, the yield strengths are very close to each other (within 6%) for all three volume fractions. After the yield point, the hardening effect is observed to be higher

than that of the primitive lattices, with the stress values increasing with the increase in volume fraction. The densification after a 40% strain value is observed in gyroid lattices too. However, the difference between the curves of different volume fractions is not as high as seen in the primitive lattice. In the case of the compression test of Gyroid 40%, the limit of the compression testing machine was reached at 245 kN and 25% strain. Therefore, the test had to be stopped at that value.

3.3 FEA results with and without residual stresses

Self-contact and densification increase the required computation power and the time for the simulation multi-fold. Also, the gyroid 40% specimen could be compressed to a maximum of 25% strain only (see Section 3.2). Therefore, considering these constraints, simulations were carried out only until 20% strain and compared to the experimental compression data in this strain region. Representative images of the displacement and equivalent stress at 20% strain compression simulation for the 20% volume fraction of primitive and gyroid are shown in Figure 8.

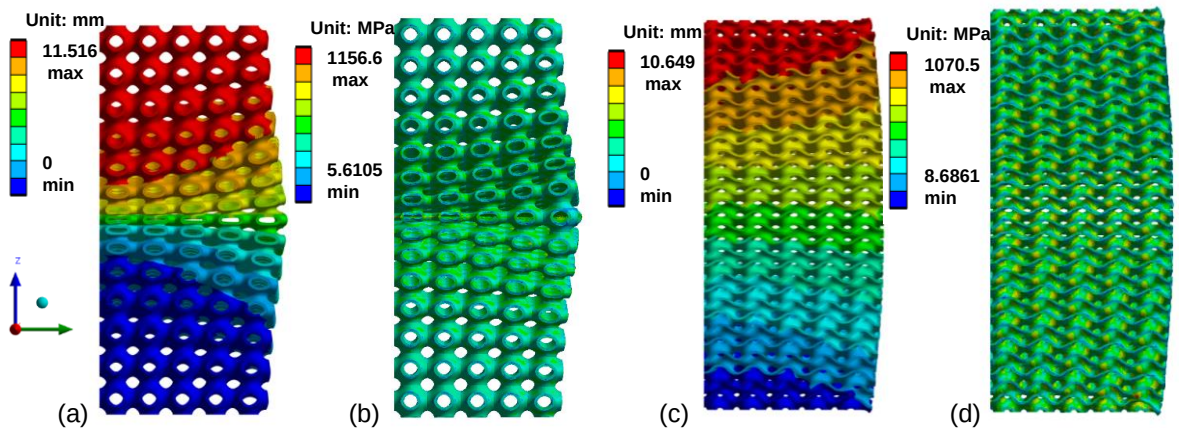

Figure 8: (a) Deformation and (b) stress distribution in the quarter primitive 20 and (c) deformation and (d) stress distribution in the quarter gyroid 20 specimen post compression

Even after compression to 20% only, the simulation results show high similarities with the experimental result seen in Figure 7, by showing significant bulging in the central region along the height of the model (along the Z axis). Also, the unit cell walls are closer to each other at the center (around the Z axis), and the distance increases towards the outer region, creating a fan-like structure, mimicking the experimental results. This deformation pattern is similar to that observed in the literature in [18] and [3]. This pattern leads to the formation of diagonal shear bands in the uniform wall thickness lattice structures as shown in the above studies.

The stress-strain curves for the 20, 30, and 40% volume fraction primitive structure for the three categories, namely experimental, simulation without residual stresses (without RS) and simulation with residual stress consideration (with RS) are shown in Figure 9. It can be observed from the graphs that there is a noticeable difference between the stress-strain curves of the experiments and the compression test simulation without RS. The stress-strain curves of the experimental data and simulation with RS have values lower than that of the simulation without

RS. Therefore, it can be said that the simulation results agree with the experimental data, and the RS present in the specimen negatively affect the compressive properties. Similar stress-strain curves for the gyroid structures with 20, 30, and 40% volume fractions are shown in Figure 10. For gyroid structures also, differences can be observed in the stress-strain curves of simulation without RS, simulation with RS and experimental data. Also, in the case of the gyroid, the curves of simulation without RS are higher than the other two. As seen in Figure 5, the as-built specimen already contains accumulated RS from the AM process and therefore, the yield strength is reached earlier during compression. Therefore, it confirms that the RS reduce the compressive strength of the lattice structures.

It is important to note that in the case of primitive 20, the softening behavior observed in the experimental data shortly after the yield is predicted more extremely by the simulation with RS. This is similar to the observation made by Ahmed et al. where softening is seen prominently in primitive lattices with a volume fraction of 10%. It can be associated with localized deformation and buckling of TPMS walls [12]. The wall thickness of the simulation model is less than that of the fabricated model, which leads to more localized deformation and higher softening behavior in the simulation with RS than in the experiments. A similar pattern is seen in a study by Zhang et al. [3], where a primitive structure shows softening behavior after the end of the elastic region, while the gyroid structures show continuous hardening behavior. According to [3], this stress-strain response is dependent on the micro-architecture of the structures, and the softening in primitive structures is due to local buckling of curved cell walls.

However, unlike the primitive structures, in the gyroid, the stress values of the experimental data are higher than that of the simulation with RS data, though the paths followed are very similar. A possible explanation for this behavior could be the additional mass of the gyroid experimental specimens as compared to the simulation model. As discussed earlier, the weight difference between the simulation model and the fabricated specimen is nearly 16%. Also, the weight of the gyroid structure is higher than that of the primitive one (11%), which is responsible for the higher difference in the simulation with RS and experimental curves in the gyroid compared to primitive structures. As the weight difference reduces with increasing volume fraction, these curves get closer to each other.

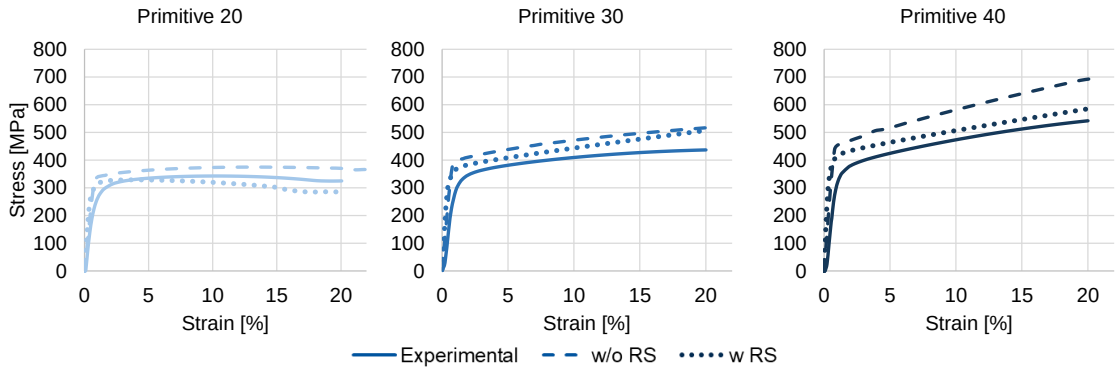

Figure 9: Stress strain graphs for the compression tests and simulation of primitive TPMS with residual stress (w RS), without residual stress (w/o RS)

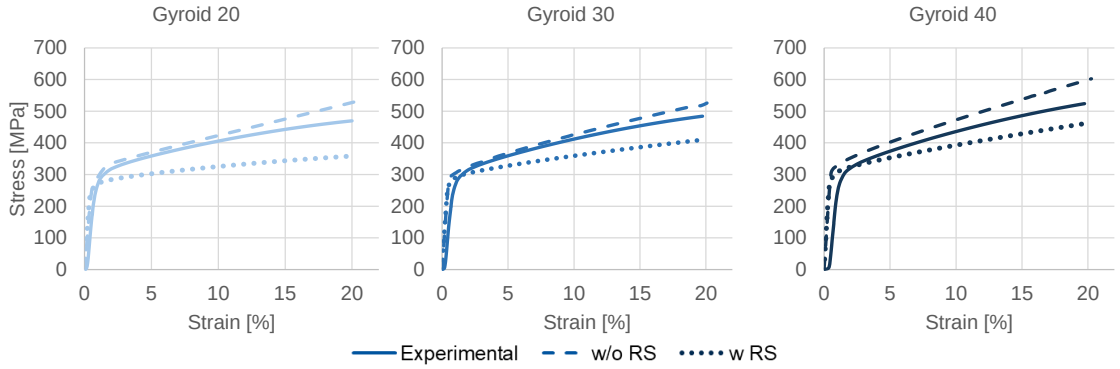

Figure 10: Stress strain graphs for the compression tests and simulation of gyroid TPMS with residual stress (w RS), without residual stress (w/o RS)

Young's modulus was calculated from the slope of the curve in the elastic region and the 0.2% yield method was used to calculate the yield strength. The graphical representation of values for the experimental compression tests, simulation with RS, and simulation without RS for the primitive and gyroid structure is shown in Figure 11. It can be seen from the graph for primitive that both Young's modulus and yield strength for the primitive lattice increase with increasing volume fraction. The simulation results with and without RS follow a trend similar to the experiments. Also, it can be observed that the values of Young's modulus and yield strength are lowest for the experimental data, and highest for the simulation without RS. Therefore, it can be inferred that the RS reduce Young's modulus and yield strength for the primitive lattice structure. It can be seen from the graph that for the gyroid lattice, the value of Young's modulus from the simulation does not vary to a large extent with the change in volume fraction. Also, Young's modulus values from the simulation with RS are lower than that of the simulation without RS, but only by a very small margin. Compared to that, the experimental values show a large decline when compared to the simulations. The yield strength values show that the yield strength of the gyroid lattice increase with the increasing volume fraction, though the increase is not as sharp as compared to the primitive. In this case also the yield strength values of the experimental data and simulation with RS are lower than that of the simulation without RS. Also, the experimental data and simulation with RS data match very closely.

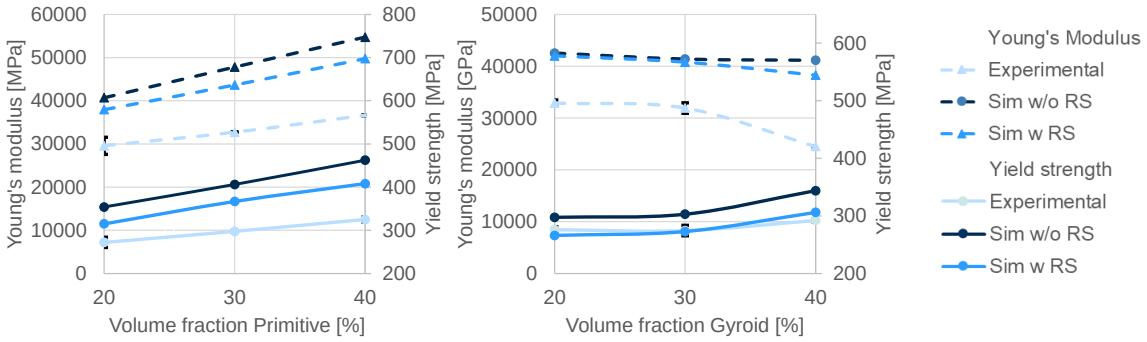

Figure 21: Young's modulus and yield strength for primitive and gyroid lattices

These observations agree with the findings from [12] where the effect of RS is notable, especially under compression loading. The softening effect on the lowest volume fraction of primitive lattice is also observed in that study. It also mentions that the RS have little effect beyond the yield region, which is also seen here, that after the yield, the curves follow a similar path.

SEA is defined as the energy absorbed by the material under uniaxial compression normalized by its density up to the point of densification. In this paper, SEA is calculated by calculating the area under the stress-strain curve and dividing it by the volume fraction value. As the simulation was performed up to 20% strain, that point was considered for the SEA calculation. However, for more effective utilization of the SEA, the complete range should be considered.

The graphical representation of these values for primitive and gyroid is shown in Figure 12. It can be seen from the graph that for both primitive and gyroid, the SEA values decrease with increasing volume fraction. When compared volume fraction-wise, the SEA of the gyroid for 20% volume fraction is higher compared to the primitive. However, this is an outlier from the other two volume fractions. The primitive 20 lattice shows significant softening behavior shortly after the yield. This leads to a decrease in the area under the stress-strain curve, leading to a decrease in SEA value. For volume fractions 30 and 40%, both primitive and gyroid show hardening behavior, but the SEA values of primitive are observed to be higher. [18] compared the energy absorption of the uniform sheet (US) and functionally graded (FG) TPMS lattices, and found that for the effective use of TPMS lattices as energy absorbers, FG lattices are a better alternative, as they absorb a total cumulative 60% more energy.

As these values are calculated from the stress-strain data, the trend regarding values of experiments, with RS and without RS is followed. For both primitive and gyroid, the SEA values without RS are higher than that of experimental values and with RS values up to 20% strain.

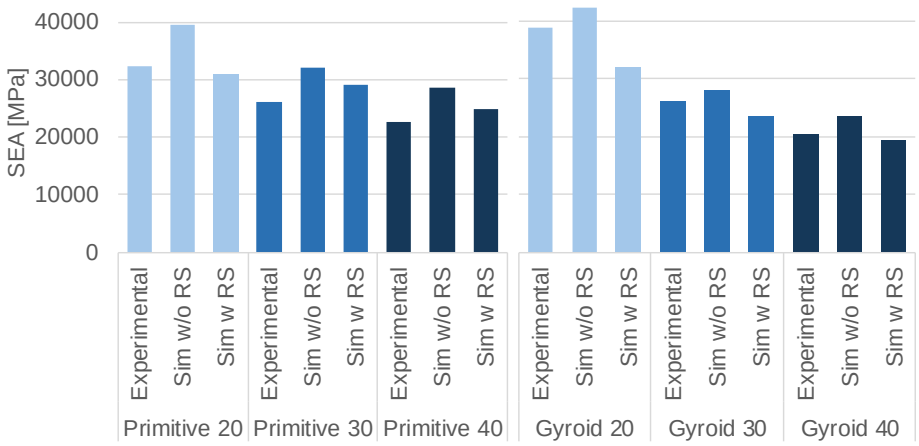

Figure 32: Specific energy absorption for primitive and gyroid lattice

As a summary, it can be said that the RS, which result from non-uniform thermal expansion and contraction during the PBF-LB/M process, adversely affect the performance of the lattice

structure specimens. Specifically, the presence of RS within the component lead to a reduction in its compressive yield strength. The compressive nature of these RS adds to the compressive load applied to the specimens, reducing their ability to withstand compressive forces. As a result, the compressive yield strength, Young's modulus and SEA of the specimens are compromised, highlighting the critical role of the RS in influencing the overall mechanical behavior and performance of lattice structures manufactured using PBF-LB/M.

4 CONCLUSION AND OUTLOOK

The effect of RS on the key mechanical properties: yield strength, Young's modulus and SEA of three volume fractions (20, 30 and 40%) of primitive and gyroid TPMS lattice structures is studied in this paper.

The simulation results of yield strength, Young's modulus and SEA with RS better represent the experimental results, which show lower values than those calculated from the simulations without RS. Therefore, it can be concluded that modeling with RS can well represent the degrading effect on the mechanical properties of additively manufactured lattices. Thus, the sequential thermal structural approach to account for the RS and use it for further simulation is effective and can be used for other lattices or AM parts.

The primitive 20% specimen shows significant softening, which is not shown by any other tested specimens. Both the Young's modulus and yield strength of primitive increases with the increasing volume fraction. Whereas for the gyroid, yield strength increases but the Young's modulus is in the similar value range with the increase in volume fraction. However, the detrimental effect of RS is seen to be consistent.

The detrimental effect of RS on SEA is also seen up to a compression of 20%. The conclusion regarding SEA can be more complete if studies for complete strain range including self-contact and densification are considered.

These findings are important as the RS have a very significant effect on the fatigue life and crack propagation etc. of additively manufactured parts. Further investigation regarding the effect of scanning strategies and post-heat treatment on the RS and mechanical properties, and the effect of RS on other lattices and in general AM parts can be conducted.

REFERENCES

[1] C. Pan, Y. Han, and J. Lu, "Design and Optimization of Lattice Structures: A Review," *Applied Sciences*, vol. 10, no. 18, p. 6374, 2020, doi: 10.3390/app10186374.

[2] J. Mueller, K. H. Matlack, K. Shea, and C. Daraio, "Energy Absorption Properties of Periodic and Stochastic 3D Lattice Materials," *Adv. Theory Simul.*, vol. 2, no. 10, p. 1900081, 2019, doi: 10.1002/adts.201900081.

[3] L. Zhang *et al.*, "Energy absorption characteristics of metallic triply periodic minimal surface sheet structures under compressive loading," *Additive Manufacturing*, vol. 23, pp. 505–515, 2018, doi: 10.1016/j.addma.2018.08.007.

[4] X. Lu, M. Cervera, M. Chiumenti, and X. Lin, "Residual Stresses Control in Additive Manufacturing," *JMMP*, vol. 5, no. 4, p. 138, 2021, doi: 10.3390/jmmp5040138.

[5] M. Strantza *et al.*, "Effect of the scanning strategy on the formation of residual stresses in additively manufactured Ti-6Al-4V," *Additive Manufacturing*, vol. 45, p. 102003, 2021, doi: 10.1016/j.addma.2021.102003.
[6] W. Chen *et al.*, "Microscale residual stresses in additively manufactured stainless steel," *Nature communications*, vol. 10, no. 1, p. 4338, 2019, doi: 10.1038/s41467-019-12265-8.
[7] P. J. Withers and H. Bhadeshia, "Residual stress. Part 1 – Measurement techniques," *Materials Science and Technology*, vol. 17, no. 4, pp. 355–365, 2001, doi: 10.1179/026708301101509980.
[8] T. Fritsch *et al.*, "On the determination of residual stresses in additively manufactured lattice structures," *Journal of applied crystallography*, vol. 54, Pt 1, pp. 228–236, 2021, doi: 10.1107/S1600576720015344.
[9] T. Mukherjee, W. Zhang, and T. DebRoy, "An improved prediction of residual stresses and distortion in additive manufacturing," *Computational Materials Science*, vol. 126, pp. 360–372, 2017, doi: 10.1016/j.commatsci.2016.10.003.
[10] M. Gan, Q. Wu, and L. Long, "Prediction of Residual Deformation and Stress of Laser Powder Bed Fusion Manufactured Ti-6Al-4V Lattice Structures Based on Inherent Strain Method," *Mat. Res.*, vol. 26, 2023, doi: 10.1590/1980-5373-MR-2022-0516.
[11] K. Bruggeman, "Simulation of residual stress generation in additive manufacturing of complex lattice geometries," WRIGHT STATE UNIVERSITY, 2022.
[12] N. Ahmed, I. Barsoum, and R. K. Abu Al-Rub, "Numerical Investigation on the Effect of Residual Stresses on the Effective Mechanical Properties of 3D-Printed TPMS Lattices," *Metals*, vol. 12, no. 8, p. 1344, 2022, doi: 10.3390/met12081344.
[13] Ansys, *Ansys print and science calibration guide: Help document.* [Online]. Available: https://ansyshelp.ansys.com/account/secured?returnurl=/Views/Secured/corp/v231/en/add_cal/add_cal_quick_start.html
[14] O. Al-Ketan, R. Rowshan, and R. K. Abu Al-Rub, "Topology-mechanical property relationship of 3D printed strut, skeletal, and sheet based periodic metallic cellular materials," *Additive Manufacturing*, vol. 19, pp. 167–183, 2018, doi: 10.1016/j.addma.2017.12.006.
[15] Y. Liu, Y. Yang, and Di Wang, "A study on the residual stress during selective laser melting (SLM) of metallic powder," *Int J Adv Manuf Technol*, vol. 87, 1-4, pp. 647–656, 2016, doi: 10.1007/s00170-016-8466-y.
[16] S. Goel *et al.*, "Residual stress determination by neutron diffraction in powder bed fusion-built Alloy 718: Influence of process parameters and post-treatment," *Materials & Design*, vol. 195, p. 109045, 2020, doi: 10.1016/j.matdes.2020.109045.
[17] L. A. Parry, I. A. Ashcroft, and R. D. Wildman, "Geometrical effects on residual stress in selective laser melting," *Additive Manufacturing*, vol. 25, pp. 166–175, 2019, doi: 10.1016/j.addma.2018.09.026.
[18] M. Zhao, D. Z. Zhang, F. Liu, Z. Li, Z. Ma, and Z. Ren, "Mechanical and energy absorption characteristics of additively manufactured functionally graded sheet lattice structures with minimal surfaces," *International Journal of Mechanical Sciences*, vol. 167, p. 105262, 2020, doi: 10.1016/j.ijmecsci.2019.105262.